Turkish Online Journal of Qualitative Inquiry (TOJQI)
Volume 12, Issue 7, July 2021: 9910 - 9927

Research Article

Performance Improvement of Grid-Connected DFIG based Wind Energy Conversion System in Subsynchronous Operation using Adaptive Control

Abrar Ahmed Chhipa[1], Vinod Kumar[2] and Prashant Kumar[3]

Abstract

This study proposes a adaptive controller for the reduce the subsynchronous resonance (SSR) for grid-connected DFIG based wind energy conversion system considering the small signal effect of rotor side converter (RSC) and grid side converter (GSC). For analysis of SSR considering different operating conditions such as varying wind speed and compensation level, a unique mathematical model of DFIG based windfarms presents in state space model. The model includes subsystems such as wind turbine, DFIG, series compensated grid connected line and novel Rotor Side Converter RSC-GSC model. The time domain analysis for SSR and and the effective SSR damping control technique is built in MATLAB/SIMULINK. This technique avoids the addition of extra SSR Damping Controller (SSRDC) and use an efficient Fuzzy Logic Controller (FLC) based single controller for RSC. This controller is an effective dual-purpose controller and is utilizes for power control of the WECs as well as for damping the torque due to SSR. Simulation results shows in dynamic condition electromagnetic torque oscillation reduces significantly compares to conventional control. The FLC posses high disturbance rejection capabily.

Keywords: *wind energy conversion system, DFIG, fuzzy logic control, subsynchronous resonance, damping controller.*

Introduction

The continuously increasing usage of fossil fuels has adversely affected the economic growth of developing countries. Therefore, it has become the need to increase the use of renewable energy resources for electricity generation. The renewable energy sources such as solar, wind energy, etc., are clean, surplus in amount and available for free of cost. Hence, the renewable energy sources are bridging the energy gap. Out of all other renewable energy sources, wind energy has seen a vast growth in green engineering. The cost of electricity from wind has reduced in the past years with the advancements of technology. The WECs is widespread all over the world [1-2]. In the last few decades, research was going on to improve the penetration of renewables into the power system. Hence, it is essential to explore the interconnection of the wind farm to the grid/load centers and their related issues.

The global cumulative wind installed capacity is reached 733.28 GW by the end of year 2020. In the last two decays, it increases from 16.93 GW to 7333.28 GW, a 4231.25% increase as shown in Fig. 1 [3].

Among the top ten wind installed capacity countries, India holds the fourth position after China, the USA and Germany by the end of the year 2020 with 38.56 GW installed capacity, as shown in Fig. 2. China alone holds a capacity of 281.99 GW, which is 7.3 times that of India. The market outlook for

the global wind industry remains positive. The global wind energy market is expected to grow on average by 4 per cent each year, even though the installed capacity for 2020 marked a new high [4].

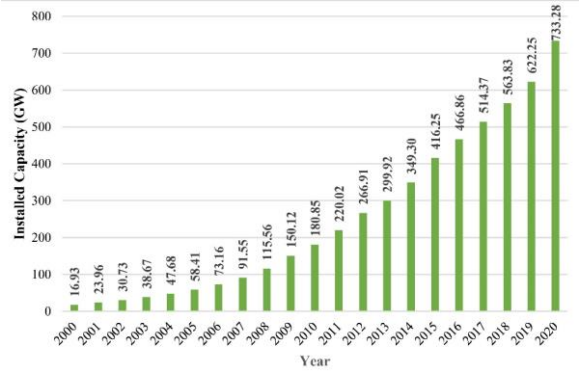

Figure 1. Global Cumulative Wind installed capacity during 2000-2020

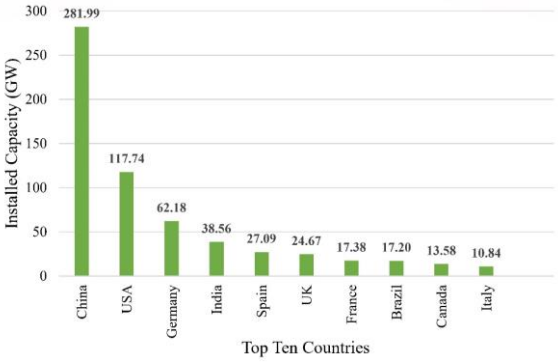

Figure 2. Country ranking of Wind Installed Capacity, end of 2020

In India, wind power accounted for two-thirds of the renewable energy installed capacity. India's total wind turbine installed capacity is around 38.56 GW up to 2020 as shown in Fig. 3. The government aims to achieve 227 GW of renewable energy capacity (including 114 GW of solar capacity addition and 67 GW of wind power capacity) by 2022, more than its 175 GW targets as per the Paris Agreement. The government plans to establish a renewable energy capacity of 523 GW (including 73 GW from Hydro) by 2030 [2].

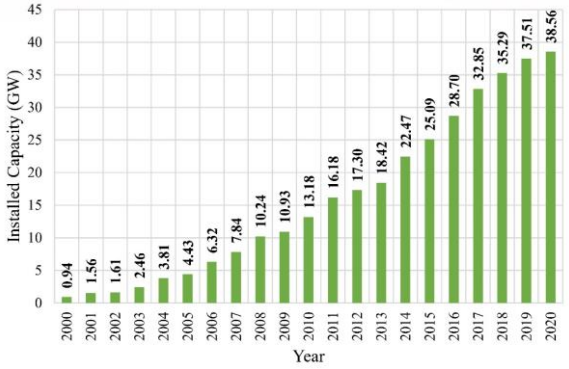

Figure 3. Total wind turbine installed capacity in India from 2000 to 2020

The Subsynchronous Resonance (SSR) phenomenon is a state in which the electrical network interchanges the energy between the mechanical and electrical systems [5-6]. The system becomes oscillatory at a frequency equal to the natural frequencies. The natural frequencies are below the system synchronous fre quency [7-8]. This phenomenon is the resonance in the electrical system which is resulted by the insertion of capacitive compensation. The electrical resonance frequency of the system shown in Fig.4 is given in equation (1)

$$f_{res} = f_s \sqrt{\frac{X_C}{X_C + X_L + X_{sys}}} \tag{1}$$

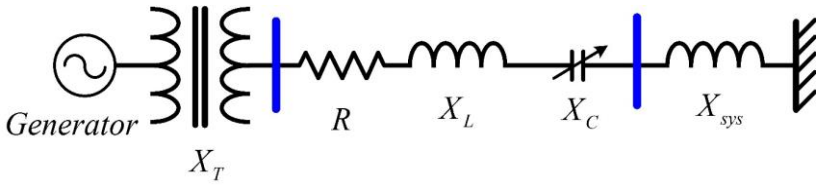

Figure 4. Single line diagram of Grid connected electrical network

The phenomenon of resonance may lead to various power system issues such as instability, electrical torque and power oscillations, turbine-generator shaft fatigue, etc.[9-10]. Therefore, a detailed investigation of SSR oscillations is required in the WECs studies. Also, the research on effective mitigation techniques of these SSR oscillations are important.

The SSR can cause different effects on the systems which are mainly classified into three types named as Torsional Interactions (TI), Induction Generator Effect (IGE) and Torque Amplification (TA).

Based on the time required for the SSR oscillations to grow, it is classified into steady state and transient SSR. IGE and TI are classified under steady state SSR. whereas, TA is derived from transient SSR. Transient SSR occurs due to a large disturbance in the system.

The damping of SSR oscillations is a very big challenge in WECs. Many papers have investigated the effect of SSR on SCIG based windfarms [11]. As the state of art WPP uses DFIG based generator, the investigations on the effect of wind turbines on damping SSR is very important [12]. The torsional interactions and their remediation for various WPPs are reported in [13], which can help in exploring the damping of SSR.

The literatures show varied research on damping of SSR oscillations in SCIG using FACTS devices. From these literatures, it is inferred that additional SSR damping controller (SSRDC) is required along with the FACTS controllers for damping oscillations due to SSR. Additional controller may complicate the entire system and make it bulky and inefficient. Recently, due to wide variations in speed and the presence of readily available converters, DFIG has become more popular, in order to protect the DFIG system from torsional interactions, the efficient damping controller has to be developed. Hence the SSR oscillation investigator group started focusing on the analysis of SSR and its damping on DFIG based wind system.

The SSR damping of a series compensated DFIG based windfarm is proposed in [14] with the help of a controller incorporated along with the GCSC. The drawback is that this proposed model has DFIG's converter controllers and also a separate controller for the SSR damping in GCSC. Practically, the decoupling of these controllers is not possible. Hence it may lead to the negative damping of the SSR oscillations. The distance between the torque sensor and the voltage across series capacitor may lead to delayed SSR damping.

Most of the controllers used for SSR damping are linear controllers [15-17]. The performance of these controllers are poor under fast dynamic conditions. Most of the literatures reported the system model of DFIG based wind farm without considering the dynamics of RSC and GSC. The RSC and GSC of the DFIG system are considered as constant voltage source models. It has been observed that the dynamics of these converters largely effects the stability of the system. In this work, the small signal model of RSC and GSC is developed and integrated to the system model for the complete SSR analysis. The stability of the complete system including RSC and GSC is analyzed for different operating conditions.

The oscillations due to SSR can be damped by connecting SSRDC. Most of the literatures reported the design of a separate SSRDC in DFIG based wind farms which can cause instability in the system due to the interactions between other controllers [5]. The RSC and GSC works independently to control active an reactive for power for the grid synchronization [8]. The proposes control technique control the damping oscillations due to SSR frequencies. Since the SSR frequencies are different from the

system operating frequencies, a completely decoupled SSR control is possible with the same existing controller of RSC-GSC. The proposes technique is cost-effective as it does not require additional SSRDC for the control of SSR.

Conventional controllers like PI controllers are commonly used for damping of SSR oscillations. Under fast dynamic conditions, these controllers are failed to give the required performance. A fuzzy based controller is proposed in this research work which can easily adapt to the changes in the operating conditions like wind speed variation and the capacitor compensation level variation of the transmission line.

System Modeling for Subsynchronous Resonance Analysis

This section presents the detailed mathematical modelling of the series compensated grid-connected DFIG based WTGs. To conduct a stability analysis on the proposed system, a detailed state space modelling of the proposed system is developed. The complete system under study is divided into different subsystems representing wind turbine, DFIG, series compensated transmission line, RSC-GSC converter model and etc., Then the individual subsystems are integrated together to formulate the complete system. The main novelty in this modelling is the incorporation of RSC-GSC dynamics into the main system. By including the dynamics of RSC-GSC in the main system, the SSR analysis is more accurate.

System Configuration

The system considered in this study is grid connected 2MW WEGs connected to the grid through the long transmission line and its schematic is shown in Fig.5. The specifications of the 2MW WTG is given in Table 1. The proposed system consists of multiple subsystems such as wind turbine, DFIG machine, series compensated transmission line of inductive reactance (X_L), series compensative reactance (X_C), RSC- DC link-GSC and Grid. The transmission line reactance can be varied by varying the capacitive reactance (X_C) connected in series with the line as shown in Fig. 5. PCC in Fig. 5 is a Point of Common Coupling.

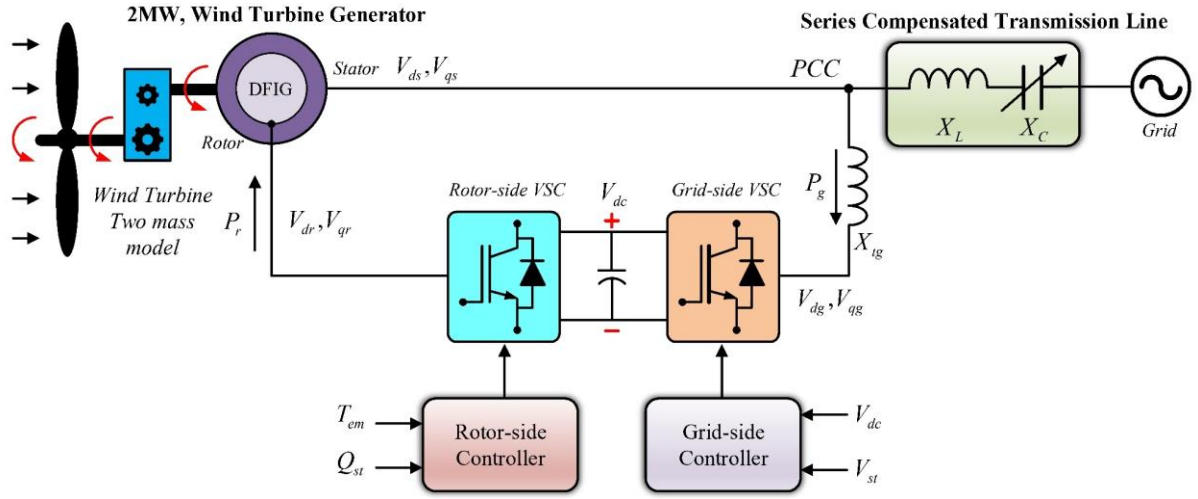

Figure 5. Proposed system

Table 1.

2MW DFIG parameters

Parameter	Value	Parameter	Value
Rated Power	2 MW	J_s	0.9 s

voltage	690V	D_{tg}	1.5 pu
X_s	0.09231 pu	X_{tg}	0.3 pu
X_r	0.09955 pu	DC link capacitor	1400 µF
R_s, R_r	0.00488 pu, 0.00549 pu	K_{tg}	0.5 to 50 pu
X_L	0.5 pu	V_{dc}	1200 V
J_t	4.29 s		

Modeling of DFIG

A 2MW DFIG based WTG parameters are considered. The stator and rotor currents are chosen as state variables. Wind turbine is coupled with the DFIG through the shaft section. The assumptions are made in the modelling are, (a) The effect of hysteresis and magnetic saturation are neglected, (b) Symmetrical Stator and rotor parameters are considered and (c) The capacitance of the windings is neglected. The equivalent circuit of the DFIG is given in Fig. 5.

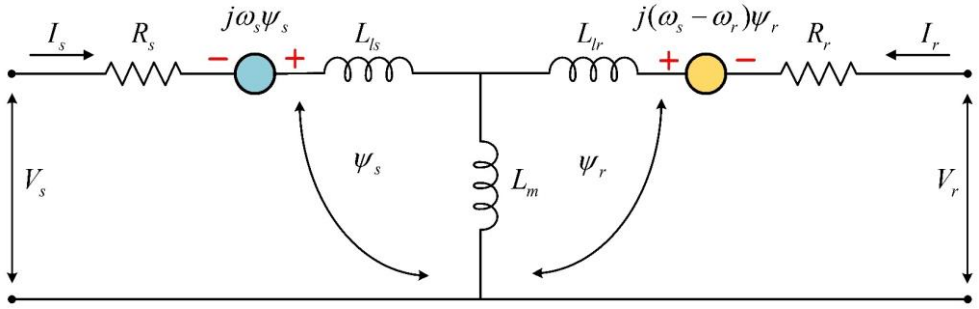

Figure 5. Equivalent circuit of DFIG

For the steady state analysis, derivatives of flux linkages are equal to zero. Whereas for the dynamic analysis, derivatives of flux linkages are considered. The magnetization circuit is represented by the shunt inductance L_m by neglecting R_0. The stator and rotor voltages are transformed from abc to synchronously rotating *dq* frame and are described by equation from (2) to (5).

$$V_{ds} = -R_s i_{ds} + \frac{1}{\omega_s}\frac{d}{dx}\psi_{ds} - \psi_{qs} \tag{2}$$

$$V_{qs} = -R_s i_{qs} + \frac{1}{\omega_s}\frac{d}{dx}\psi_{qs} - \psi_{ds} \tag{3}$$

$$V_{dr} = -R_r i_{dr} + \frac{1}{\omega_s}\frac{d}{dx}\psi_{dr} - \psi_{qr} \tag{4}$$

$$V_{qr} = -R_r i_{qr} + \frac{1}{\omega_s}\frac{d}{dx}\psi_{qr} - \psi_{dr} \tag{5}$$

Where $s = \omega_s - \omega_g / \omega_s$, $s\omega_s = \omega_s - \omega_g$ and $\omega_s - s\omega_s = \omega_g$

The flux linkages are given by equations (6) to (9).

$$\psi_{ds} = -(X_s i_{ds} + X_m i_{dr}) \tag{6}$$

$$\psi_{qs} = -(X_s i_{qs} + X_m i_{qr}) \tag{7}$$

$$\psi_{dr} = -(X_r i_{dr} + X_m i_{ds}) \tag{8}$$

$$\psi_{qr} = -(X_r i_{qr} + X_m i_{qs}) \tag{9}$$

Rearranging and linearizing equation from (2) to (9), the state space matrix is give by equation (10)

$$\left[\dot{X}_{DFIG}\right]=\left[A_{DFIG}\right]\left[X_{DFIG}\right]+\left[B_{DFIG}\right]\left[U_{DFIG}\right] \tag{10}$$

Where

$$[A_{DFIG}]=\begin{bmatrix} \frac{-R_s\omega_s X_r}{-X_m^2+X_rX_s} & \frac{\omega_s X_rX_s-X_m^2\omega_s+X_m^2\omega_{g0}}{-X_m^2+X_rX_s} & \frac{R_r\omega_s X_s}{-X_m^2+X_rX_s} & \frac{\omega_{g0}X_mX_r}{-X_m^2+X_rX_s} \\ -\frac{\omega_s X_rX_s-X_m^2\omega_s+X_m^2\omega_{g0}}{-X_m^2+X_rX_s} & \frac{-R_s\omega_s X_r}{-X_m^2+X_rX_s} & -\frac{\omega_{g0}X_mX_r}{-X_m^2-X_rX_s} & \frac{R_r\omega_s X_m}{-X_m^2+X_rX_s} \\ \frac{-R_s\omega_s X_m}{X_m^2-X_rX_s} & \frac{\omega_{g0}X_rX_s}{X_m^2-X_rX_s} & \frac{R_r\omega_s X_s}{X_m^2-X_rX_s} & \frac{X_m^2\omega_s-\omega_s X_rX_s+\omega_{g0}X_rX_s}{X_m^2-X_rX_s} \\ -\frac{\omega_g X_mX_s}{X_m^2-X_rX_s} & \frac{-R_s\omega_s X_m}{X_m^2-X_rX_s} & -\frac{X_m^2\omega_s-\omega_s X_rX_s+\omega_g X_rX_s}{X_m^2-X_rX_s} & \frac{R_r\omega_s X_s}{X_m^2-X_rX_s} \end{bmatrix}$$

$$[B_{DFIG}]=\begin{bmatrix} \frac{X_m^2I_{qs0}+X_mX_rI_{qr0}}{-X_m^2+X_rX_s} & -\frac{\omega_s X_r}{-X_m^2+X_rX_s} & 0 & \frac{\omega_s X_m}{-X_m^2+X_rX_s} & 0 \\ -\frac{\omega_s X_rX_s-X_m^2\omega_s+X_m^2I_{qs0}}{-X_m^2+X_rX_s} & 0 & \frac{\omega_s X_r}{-X_m^2+X_rX_s} & 0 & \frac{\omega_s X_m}{-X_m^2+X_rX_s} \\ \frac{X_mX_sI_{ds0}+X_rX_sI_{qr0}}{X_m^2-X_rX_s} & -\frac{\omega_s X_m}{X_m^2-X_rX_s} & 0 & \frac{\omega_s X_s}{X_m^2-X_rX_s} & 0 \\ -\frac{X_mX_sI_{ds0}+X_rX_sI_{qr0}}{X_m^2-X_rX_s} & 0 & -\frac{\omega_s X_m}{X_m^2-X_rX_s} & 0 & \frac{\omega_s X_m}{X_m^2-X_rX_s} \end{bmatrix}$$

The state and control matrices are given by $X_{DFIG}=\begin{bmatrix} i_{ds} & i_{qs} & i_{dr} & i_{qr}\end{bmatrix}^T$ and $U_{DFIG}=\begin{bmatrix}\omega_g & V_{ds} & V_{qs} & V_{dr} & V_{qr}\end{bmatrix}^T$ A_{DFIG} and B_{DFIG} indicate the system and control matrix of the DFIG respectively.

Modeling of the Transmission Line

The assumptions are made in transmission line modelling are, (a) the transformer leakage reactance is combined with the transmission line reactance, (b) the saturation effect of the transformer is neglected and, (c) the effect of line charging capacitance is neglected.

The stator terminals of the DFIG are connected to the grid through the capacitive compensated transmission line. The dynamic equations in *dq* frame of the series compensated transmission line are given by equations (11) to (14). Differential Equations of the series compensated transmission line are:

$$L\frac{d}{dx}i_{ld}=\frac{1}{L}V_{ds}-\frac{R}{L}i_{ld}+\omega_s i_{lq}-\frac{1}{L}V_{cd}-\frac{1}{L}V_{bd} \tag{11}$$

$$L\frac{d}{dx}i_{lq}=\frac{1}{L}V_{qs}-\frac{R}{L}i_{lq}-\omega_s i_{ld}-\frac{1}{L}V_{cq}-\frac{1}{L}V_{bq} \tag{12}$$

$$\frac{d}{dx}V_{cd}=\frac{1}{C_{series}}i_{ld}+\omega_s V_{cq} \tag{13}$$

$$\frac{d}{dx}V_{cq}=\frac{1}{C_{series}}i_{lq}-\omega_s V_{cd} \tag{14}$$

After linearizing the differential equations from (11) to (14), the state space model of series compensated line is given by equation (15)

$$\left[\dot{X}_{tl}\right]=\left[A_{tl}\right]\left[X_{tl}\right]+\left[B_{tl}\right]\left[U_{tl}\right] \tag{15}$$

Where

State matrix is $[A_{tl}]=\begin{bmatrix} -R/L & \omega_s & -1/L & 0 \\ -\omega_s & -R/L & 0 & -1/L \\ 1/C_{series} & 0 & 0 & \omega_s \\ 0 & 1/C_{series} & -\omega_s & 0 \end{bmatrix}$ and control matrix is $[B_{tl}]=\begin{bmatrix} 1/L & 0 & -1/L & 0 \\ 0 & 1/L & 0 & -1/L \\ 0 & 0 & 0 & 0 \\ 0 & 0 & 0 & 0 \end{bmatrix}$, state variable is $X_{tl}=\begin{bmatrix} i_{ld} & i_{lq} & V_{cd} & V_{cq} \end{bmatrix}^T$ and control variable is $U_{tl}=\begin{bmatrix} V_{ds} & V_{qs} & V_{bd} & V_{bq} \end{bmatrix}^T$.

A_{tl} and B_{tl} denote system and control matrix of the transmission line respectively. The network system and control variables are expressed in a rotating synchronous reference frame at a speed of ω_s (314 rad/s). As the system is considered as balanced three phase systems, the zero sequence components are neglected.

Modeling of RSC-GSC Converter

As the dynamics of RSC-GSC produces the large variations in the system, the modelling of the converter is important. The converter modelling includes the DC link voltage. Fig. 6 shows the interconnection of RSC and GSC along with the other subsystems. The dynamics of RSC-GSC converter is given by the state space equations (16) to (20) [54].

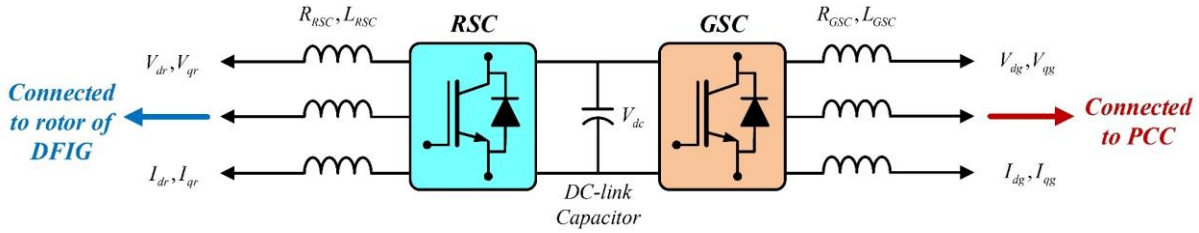

Figure 6. RSC-GSC converter

$$\frac{d}{dx}i_{dr}=\frac{-R_{RSC}}{L_{RSC}}i_{dr}+\omega_s i_{dr}-\frac{M_{dr}}{2L_{RSC}}V_{dc}+\frac{1}{L_{RSC}}V_{dr} \tag{16}$$

$$\frac{d}{dx}i_{qr}=\frac{-R_{RSC}}{L_{RSC}}i_{qr}+\omega_s i_{dr}-\frac{M_{qr}}{2L_{RSC}}V_{dc}+\frac{1}{L_{RSC}}V_{dr} \tag{17}$$

$$\frac{d}{dx}V_{dc}=\frac{-V_{dc}}{R_{dc}C_{dc}}+\frac{3M_{dr}i_{dr}}{2C_{dc}}+\frac{3M_{qi}i_{qg}}{2C_{dc}} \tag{18}$$

$$\frac{d}{dx}i_{dg}=\frac{-M_{di}}{2L_{GSC}}V_{dc}-\omega_s i_{qg}+\frac{R_{GSC}}{L_{GSC}}i_{dg}-\frac{V_{dg}}{L_{GSC}} \tag{19}$$

$$\frac{d}{dx}i_{qg}=\frac{M_{qi}}{2L_{GSC}}V_{dc}-\omega_s i_{dg}+\frac{R_{GSC}}{L_{GSC}}i_{qg}-\frac{V_{qg}}{L_{GSC}} \tag{20}$$

The model is integrated with rest of the subsystem using the following equations

$$V_{dg}=V_{ds}-X_{tg}i_{qg} \tag{21}$$

$$V_{qg}=V_{qs}+X_{tg}i_{dg} \tag{22}$$

$$i_{dg}=i_{ds}+i_{ld} \tag{23}$$

$$i_{qg} = i_{qs} + i_{lq} \tag{24}$$

Where X_{tg} is the reactance between PCC and the GSC is given in Fig 2.1.

State space equation of the RSC-GSC is given by equation (2.63) after linearizing

$$\left[\dot{X}_{BBC}\right] = \left[A_{BBC}\right]\left[X_{BBC}\right] + \left[B_{BBC}\right]\left[U_{BBC}\right] \tag{25}$$

Where $[A_{BBC}] = \begin{bmatrix} -R_{RSC}/L_{RSC} & \omega_s & -M_{dr}/2L_{RSC} & 0 & 0 \\ \omega_s & -R_{RSC}/L_{RSC} & -M_{qr}/2L_{RSC} & 0 & 0 \\ 3M_{dr}/2C_{dc} & 0 & -1/C_{dc}R_{dc} & 0 & -3M_{qi}/2C_{dc} \\ 0 & 0 & M_{di}/2L_{GSC} & R_{GSC}/L_{GSC} & -(\omega_s - X_{tg}) \\ 0 & 0 & M_{qi}/2L_{GSC} & -(\omega_s + X_{tg}) & R_{GSC}/L_{GSC} \end{bmatrix}$, $[B_{BBC}] = \begin{bmatrix} 1/L_{RSC} & 0 & 0 & 0 \\ 0 & 1/L_{RSC} & 0 & 0 \\ 0 & 0 & 0 & 0 \\ 0 & 0 & 1/L_{RSC} & 0 \\ 0 & 0 & 0 & 1/L_{RSC} \end{bmatrix}$,

$X_{BBC} = \begin{bmatrix} i_{dr} & i_{qr} & V_{dc} & i_{dg} & i_{qg} \end{bmatrix}^T$ and $U_{BBC} = \begin{bmatrix} V_{dr} & V_{qr} & 0 & V_{ds} & V_{qs} \end{bmatrix}^T$

Proposed Control Scheme

The DFIG is always embedded with the RSC and GSC controller. The proposed controller simultaneously controls the RSC and GSC for active and reactive power control for the compensation and damping. This section discussed the integration of fuzzy based RSC controllers. Traditionally, four PI controllers are required for each RSC and GSC converter. When there are high dynamic conditions, the traditional PI controller in RSC does not works effectively. It is found from the analysis that the PI gains of the RSC controllers are required to be changed manually during varying wind speed conditions. In order to design an effective controller under fast operating conditions, a Fuzzy based RSC controller is proposed and is more effective under dynamic operating conditions than PI controllers. The controller damps out the SSR oscillations effectively without the use of separate SSRDC. Also, this control scheme reduces the number of PI controllers used in RSC control. Design of the proposed controller and the system performance with this controller under different operating conditions are explained in detail in the following sections.

RSC Converter Control using Fuzzy Logic Controller

During the varying wind speed and compensation level, conventional PI controller become ineffective and need gain parameter tuning for different operating condition. Hence, to overcome such problem the Fuzzy Logic Control (FLC) is proposed. The membership functions of FLCs are derived from the design of PI controllers. The PI controller gains are tunned for different operating conditions. The input signals (error) and output signals of the PI controllers for the varying wind speed are continuously monitored with respect to its corresponding reference torque as given in Table 2.

Table 2

Operating conditions of 2MW WTG

Wind Speed (m/s)	Torque (pu)	Rotor Speed (pu)	Power (pu)
6	0.285	0.7	0.2
7	0.426	0.75	0.32
8	0.588	0.85	0.5
9	0.73	0.96	0.7
10	0.82	1.1	0.9
11	1.07	1.17	1.25

12	1.4	1.25	1.75

Variation in wind speed changes the reference toque as presented in Table 2. The PI controller-2 and PI controller 4 are manually tuned with respect to the reference torque for damping the torque oscillations. The variations in the PI gains, signals X_2, X_4, Y_2 and Y_4 in connection with PI controllers 2 and 4 are monitored for different wind speed conditions. The observed variations in the signals such as X_2, X_4, Y_2, Y_4 form the membership functions of the fuzzy controller. Two existing PI controllers (2 and 4) in the RSC controller are replaced with FLC controller. The rest of the PI controllers 1 and 2 are not to be retuned for the varying wind reference torque. While tunning the PI controller-1 and controller-2 it revealed that it does not affects the SSR oscillations. Hence, they are not replaced with FLCs. The number of basic input and output membership functions are based on wind speed variations considered for this SSR analysis. The triangular membership functions are chosen. After evaluating the signal variations for different wind speeds, PI controllers -2 and controller-4 are replaced with the FLC-B and D respectively as shown in Fig. 7 and 8. Fig 9. and 10 are the output membership functions such as V_{dr}, V_{qr} of FLC-B and D for the wind speeds of 7m/s, 8 m/s and 9 m/s.

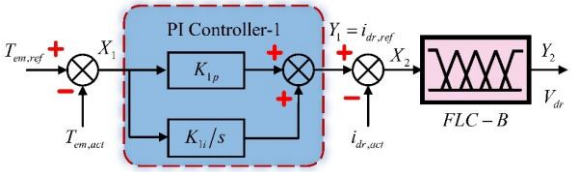

Figure 7. RSC controller loop 1 with FLC-B

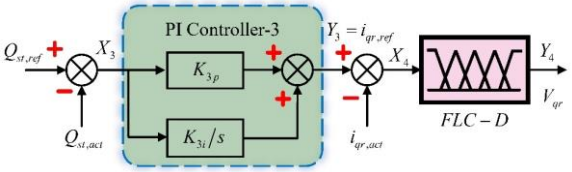

Figure 8. RSC controller loop 2 with FLC-D

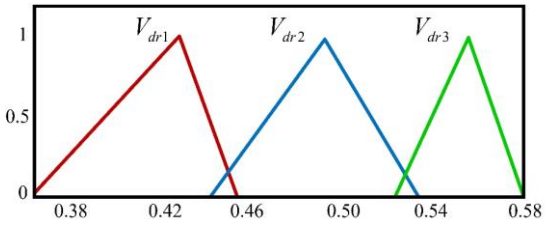

Figure 9. Output membership function of FLC-B V_{dr}

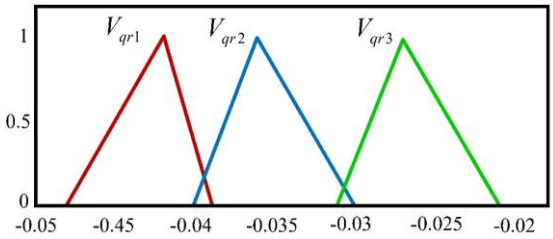

Figure 10. Output membership function of FLC-D V_{qr}

There are two types of inference systems such as Mamdani inference systems and Sugeno. Mamdani inference systems are intuitive, they have widespread acceptance and well suited for human input. Hence it can be used to model very complicated nonlinear systems. Hence, Mamdani Fuzzy inference system is used in FLC. Using Multi input multi output technique, the rules of FLC-B and D are combined together to form a single FLC (SFLC) as shown in Fig. 11.

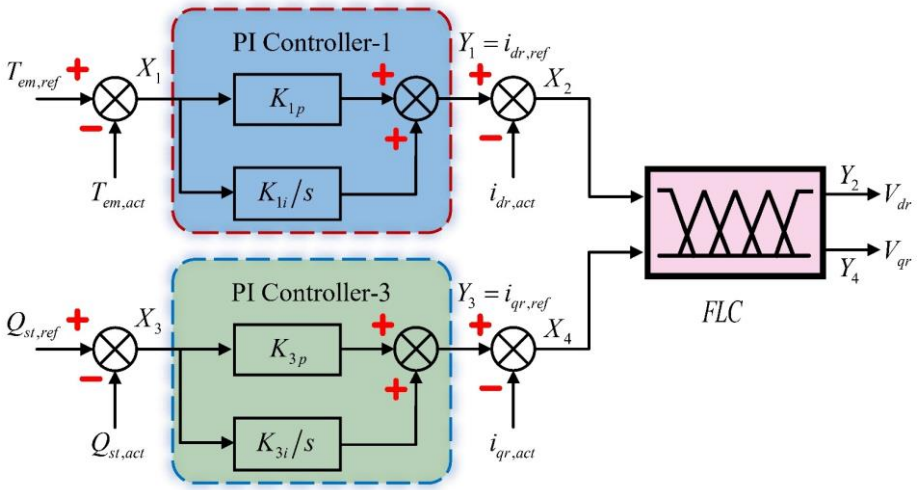

Figure 11. Fuzzy based RSC controllers.

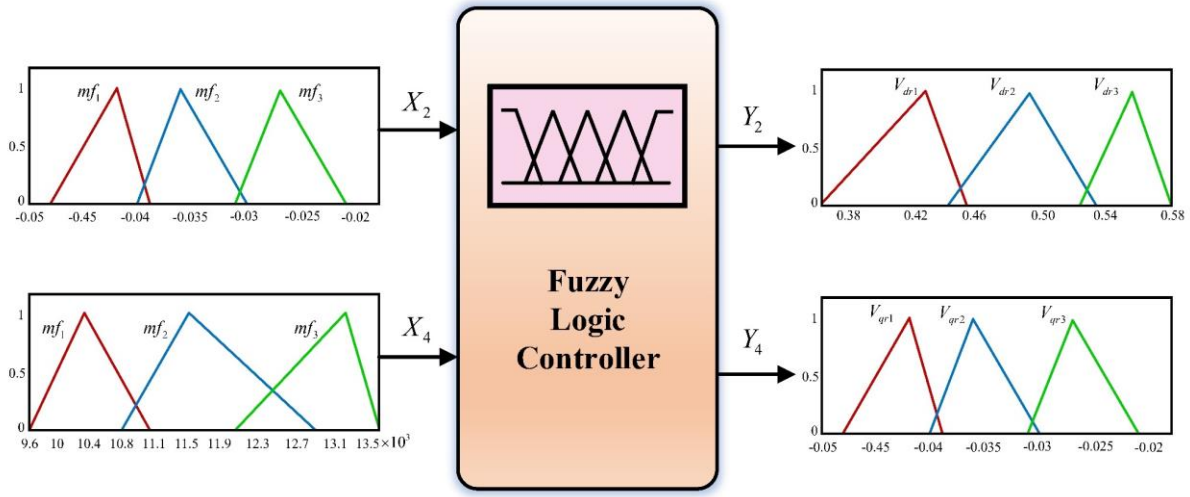

Figure 12. Single FLC controller with the membership functions.

Fig. 12 shows the multi input multi output FLC along with the membership functions. As the wind speed changes, FLC adopts the corresponding membership functions using IF-THEN rule base to inject a required rotor voltage. This is done automatically after the defuzzification for the regulation of electromagnetic torque and stator reactive power. If there is a dynamic wind speed variation, PI controller will fail to provide the proper control. Whereas, FLC responds effectively during these conditions. Also, proposed RSC-GSC converter control is well suited for grid voltage drop. The proposed controller is the modified DFIG's own RSC converter control, hence replaces PI controllers and is effective for damping out SSR oscillations in addition to its main functions such as active-reactive power compensation and grid synchronization. The separate SSRDC and individual SSR damping loop in RSC are eliminated. Table 3 describes PI and FLC controller input and output signals. The simulation results are discussed in next section.

Table 3

Input and output signals of FLC

PI	Replaced by FLC	Input Error Signals to controllers/Input membership functions	Output Signals/ membership functions
PI-2	FLC-B	$X_2 = I_{dr,ref} - I_{dr,act}$	$Y_2 = V_{dr}$

PI-4	FLC-D	$X_4 = I_{qr,ref} - I_{qr,act}$	$Y_4 = V_{qr}$

PI gain values of all the PI controllers of GSC and RSC are listed out in Table 4 and 5 respectively for different wind speed conditions. The dynamics of the generators and the electromagnetic torque oscillations are mostly involved and handled by RSC controllers, not on GSC. It is found from Table 4 that it is not necessary to adjust the PI gains of GSC controllers for the wind speeds between 7 m/s and 12 m/s. Hence, the GSC controllers are not replaced with FLC. It is perceived that there is a need to change the PI gains of PI controller 2 and 4 for the effective damping of electromagnetic torque oscillations.

Table 4

PI gains of GSC controllers

	PI- 5	**PI-6**	**PI-7**	**PI-8**
K_p	0.2	0.0001	0.08	400
K_i	0.0001	0.0001	0.0001	0.0001

Table 5

PI gains of RSC controllers

Wind Speed	**PI gains**	**PI- 1**	**PI-3**	**PI-2**	**PI-4**
7 m/s				0.01	2
8 m/s				0.02	4
9 m/s	K_p	0.05	0.05	0.03	6
10 m/s				0.03	6
12 m/s				0.03	8
7 m/s				0.001	0.001
8 m/s				0.001	0.001
9 m/s	K_i	0.001	0.001	0.002	0.002
10 m/s				0.002	0.002
12 m/s				0.002	0.002

Results and Discussion

System Performance Analysis under Steady State Operating Conditions

The steady state analysis of the integrated system is performed and the results are analysed for various operating conditions such as varying wind speed, different compensation levels, with and without RSC controllers. Fig.13 and 14 show the variation of torque and speed for a wind velocity of 8 m/s and 50% capacitive compensation level of the line. When there is no control, the system becomes unstable, and the oscillations found to be growing. With the RSC and GSC control, the torque and speed settle to its steady state value within less time.

System performance with the proposed controller is analyzed when the capacitive compensation of the line changes from 30% to 90% of X_L at the wind speed of 7 m/s. The variations of torque and speed are shown in Fig. 15 and 16 respectively. The negative torque in simulation results represents that the machine is operating in generating mode. Fig. 15 shows the electromagnetic torque oscillations for different capacitive compensation for the wind speed of 7 m/s with the proposed controller. From Fig.

15, it is noticed that, as the compensation level increases, torque oscillations magnitude is also increasing. Due to the controller action, the oscillations are kept under control but taking more time for higher compensation levels to reach steady state.

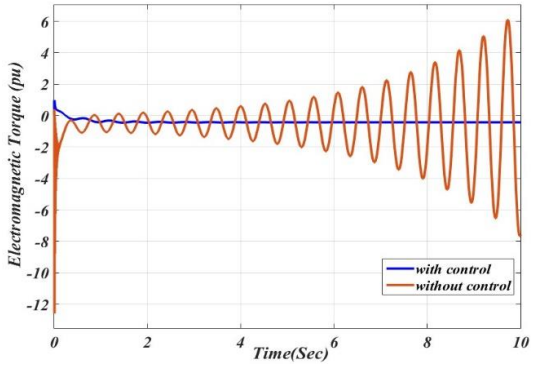

Figure 13. Variation of Electromagnetic torque oscillations (wind speed-8 m/s, 50% line compensation)

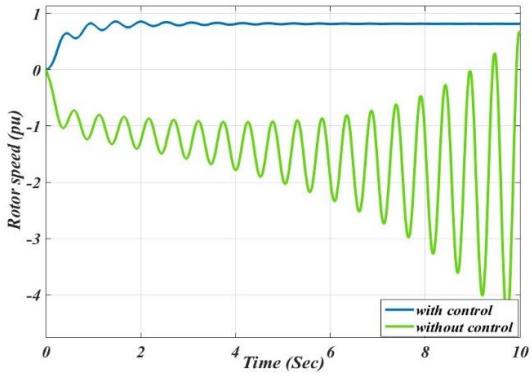

Figure 14. Variation of rotor speed (wind speed - 8 m/s. 50% line compensation)

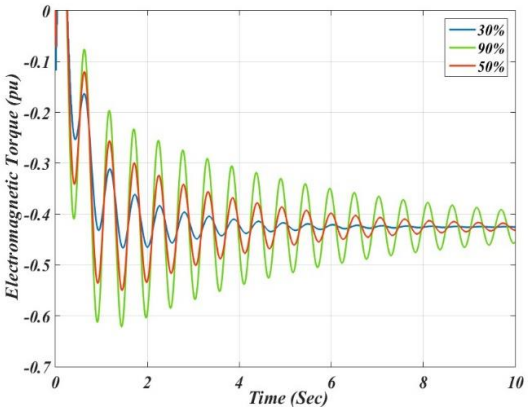

Figure 15. Variation of Electromagnetic torque (wind speed of 7 m/s)

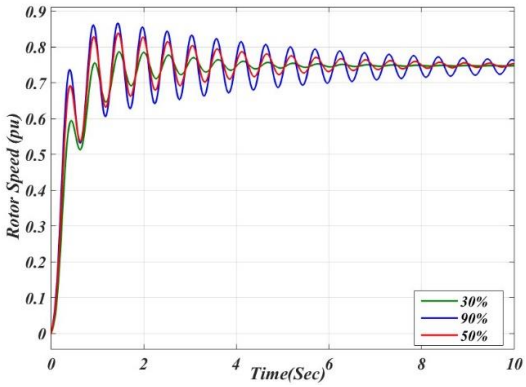

Figure 16. Variation of rotor speed for different compensation levels (wind speed of 7m/s)

Fig. 16 shows the variations of rotor speed for different capacitive compensation levels at 7 m/s wind speed. The rotor speed oscillations rise with the increase in compensation levels and the oscillations are kept under control with the action of controller. Fig. 17 to 18 show the performance of the system for a varying wind speed from 7 m/s to 9 m/s at 50% of compensation level. The controller responds faster in varying wind speed conditions. As the wind speed increases from 7 m/s to 8 m/s and to 9 m/s, the value of electromagnetic torque adapts to the value corresponds to the reference torque as shown in Fig. 17. It is detected from the Fig. 17, the amplitude of torque oscillations increases with the increase in wind speed. Similarly, the rotor speed attains the value for the varying wind speeds corresponds to maximum power conditions as per the data given in Table 2 as shown in Fig. 18.

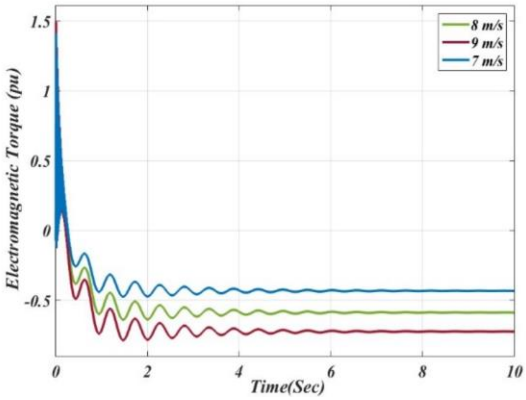

Figure 17. Variation of Electromagnetic torque for various wind speeds at 50% compensation level

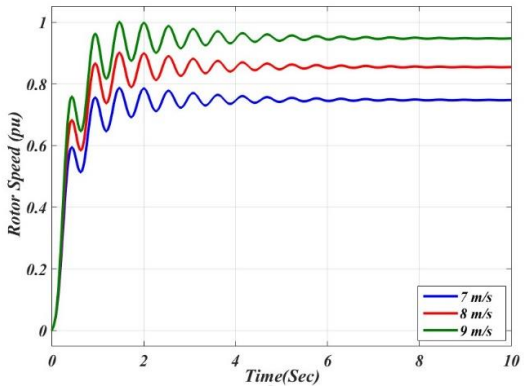

Figure 18. Rotor speed for various wind speeds

Fig. 19 and 20 show the torsional torque or twisting torque (torque between masses – turbine and generator) of DFIG for a speed of 7 m/s and 8 m/s respectively for the 50% of line compensation.

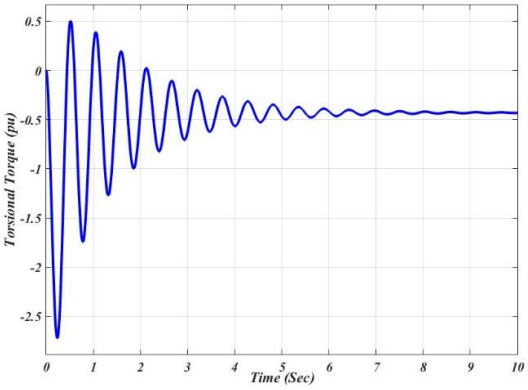

Figure 19. Variation of torsional torque (wind speed -7 m/s)

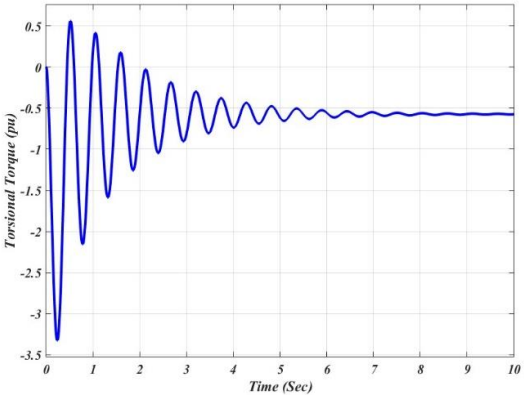

Figure 20. Variation of torsional torque (wind speed - 8 m/s)

Fig. 21 shows the variation in electromagnetic torque due to an increase in wind speed from 7 m/s to 10 m/s for a constant capacitive compensation level of 50%. It is inferred from Fig. 21 that as the wind speed increases, the variation of the initial overshoot in torque oscillations magnitude increases but settling to steady state conditions within the same time. Fig. 22 shows the variations in stator reactive power with the RSC controller. In this case, the reference value of the stator reactive power is kept as zero (Unity power factor) and it has been observed that the reactive power reaches the desired value very quickly with the help of the proposed FLC controller.

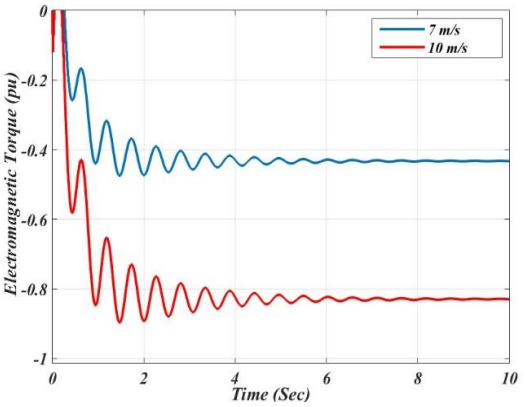

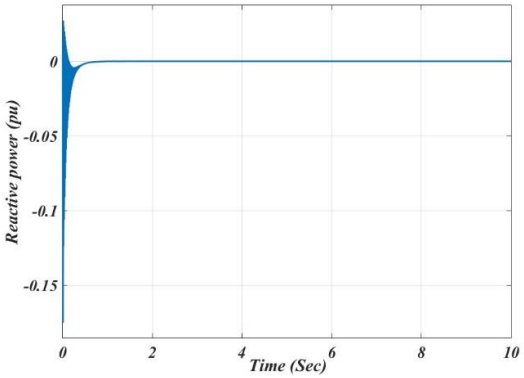

Figure 21. Variation of Electromagnetic torque for different wind speeds (50%-line compensation)

Figure 22. Variation of Stator reactive power (wind speed – 7 m/s, 50% line compensation)

The DC link voltage is regulated by the conventional PI based GSC controller. Fig. 23 shows the DC link voltage which is maintained at a constant voltage of 1200V with GSC control. Fig. 24 shows the voltage across the series capacitor which is connected in series with the transmission line, for the wind speed of 7 m/s, at 10% compensation level. An increase in the compensation level increases the voltage across the capacitor. The voltage across the series capacitor becomes unstable when there is a high compensation level 90% as shown in Fig. 25.

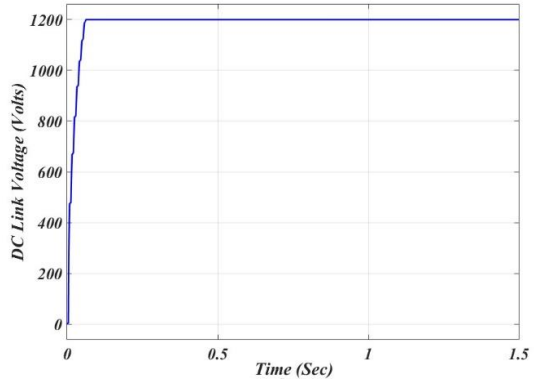

Figure 23. DC link Voltage with GSC controller

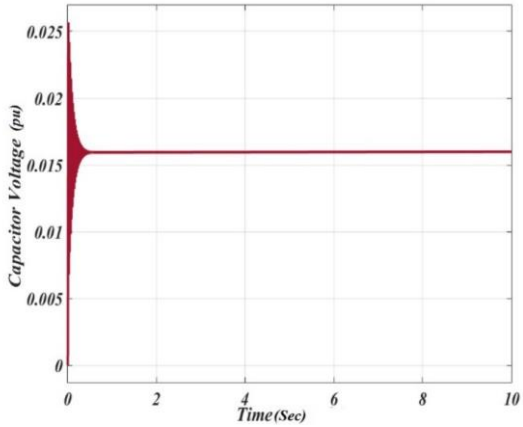

Figure 24. Voltage across the series capacitor at 7 m/s wind speed with 10% compensation

Fig. 26 and 27 show the stator voltage with 30% and 90% compensation level for the wind speed of 7 m/s respectively. When the compensation level increases, stator voltage oscillates around 1 pu and becomes unstable. Fig. 28 shows the increase in an oscillation of torque when the PI gain is improper. This result is obtained for the wind speed of 9 m/s and the compensation level of 50%. If the PI controller is not tuned properly, then the magnitude of oscillations has become high and the system moves to unstable conditions.

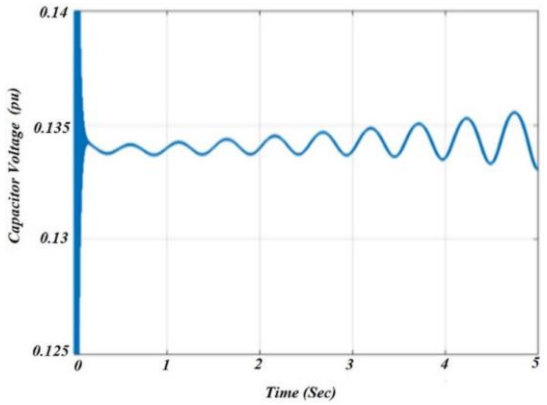

Figure 25. Voltage across the series capacitor for a speed of 7 m/s, at 90% compensation level

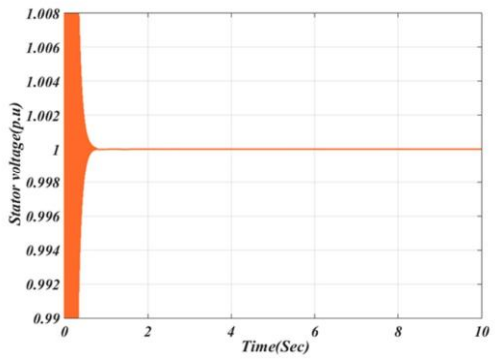

Figure 26. Variation in Stator Voltage for 30% compensation level

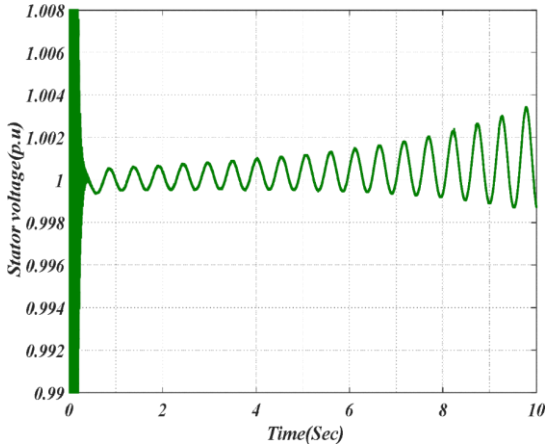

Figure 27. Variation in Stator Voltage for 90% compensation level

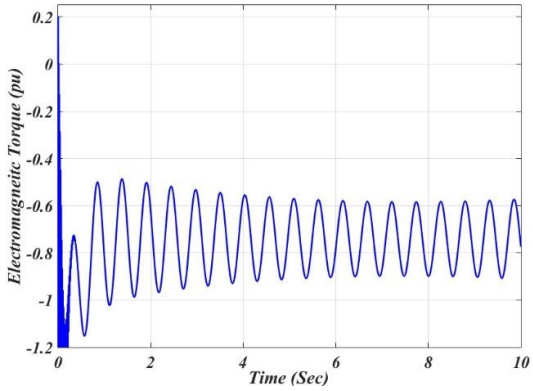

Figure 28. Variation of Electromagnetic torque (not tuned PI controller, wind speed – 9 m/s)

In all these analyses, it has been observed that by the proper control of RSC and GSC, the system can be operated in the stable conditions. A comparison of the system performance with FLC controller and PI controller is explained in next section.

System Performance Analysis under Dynamic Conditions

The performance of the system with the proposed controller is analysed under dynamic conditions. Most of the cases, under steady state conditions, the conventional PI controllers are sufficient. But when the system is undergoing fast dynamic conditions, these conventional controllers will fail to give the required performance due to poor adaptability. In such conditions, the FLC based controller performs far better than the conventional controller. In this section, the system performance is evaluated under dynamic changes. Also, the performances are compared with the PI controllers. In Fig. 29, the wind speed is varied from 7 m/s to 8 m/s then it is changed to 9 m/s at 7.5 Seconds and 15 Seconds respectively.

Fig. 30 shows the variations in electromagnetic torque and rotor speed of the turbine generator shaft for the varying wind speed pattern as shown in Fig. 29 with 50% compensation. When the wind speed varies, FLC based RSC controller parameters are tuned automatically and hence the response becomes faster. In the next case, the wind speed of the system is varied from 7 m/s to 12 m/s similar to a ramp signal. The torque oscillations of the system are compared with PI and Fuzzy based controller at 50% compensation level.

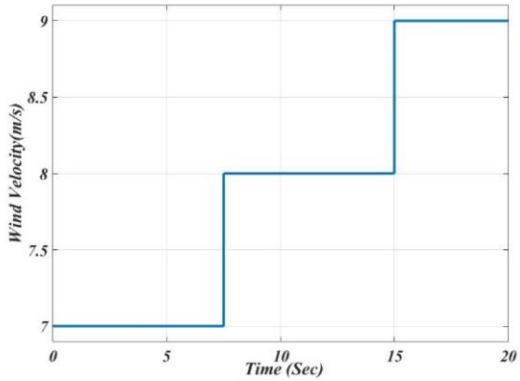

Figure 29. Variation of wind speed

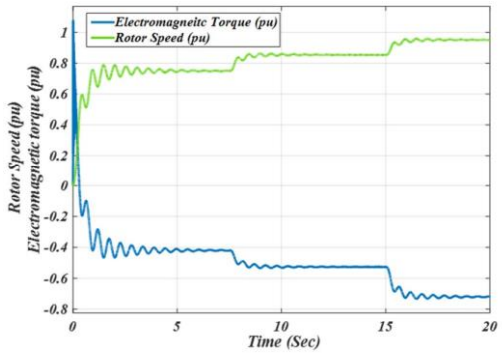

Figure 30. Variation of torque and speed for varying wind speeds

The comparison result is described in Fig. 31. As the FLC adapts the controller gain by itself, compared to PI controller, the magnitude of oscillation with FLC is lesser than PI. Fig. 32 shows the Fuzzy Vs PI controller comparison when the wind speed is changing from 7 m/s to 8 m/s in a step manner at 5 Seconds for a constant compensation level of 50%. The PI controller gain in this condition is tuned for the wind speed of 8 m/s. When the wind speed is 7 m/s till 5 Seconds, as the PI controller gains are not changed for 7 m/s, the performance of the PI is not effective till 5 Seconds. Hence, produces more torque oscillations than FLC. After 5 Seconds, the wind speed is increased to 8 m/s. As PI gains are tuned already for the wind speed of 8 m/s, the response of PI and FLC are similar. The FLC adapts the variations in the wind speed and gives the satisfactory response for both the speeds. As the grid condition changes, the system performance is affected. The performance of the controller is tested for the grid voltage variations. The results are analysed for the drop in the grid voltage under dynamic conditions. The grid voltage is dropped from 1 pu to 0.82 pu between 4 Seconds and at 6 Seconds.

Fig. 33 shows the response of electromagnetic torque oscillations with PI- based RSC and FLC based RSC under grid voltage variations at a wind speed of 7 m/s and at a compensation level of 50%. The profile of the electromagnetic torque is not affected much during the grid voltage drop between 4 Seconds and 6 Seconds by using FLC. It is detected that there is a small magnitude of overshoot in torque at 4 Seconds and 6 Seconds during grid voltage variations. With the PI-based RSC, the response is not satisfactory, as this controller takes a longer period to respond to the voltage variations. Similarly, rotor speed response with PI and Fuzzy controller is shown in Fig. 34. It is noticed that FLC provides better performance compared to the PI controller.

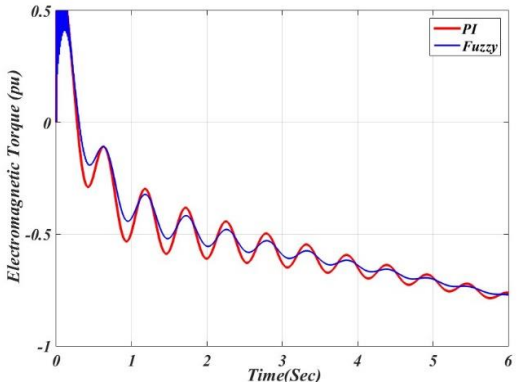

Figure 31. Electromagnetic torque for linear increase in wind speed

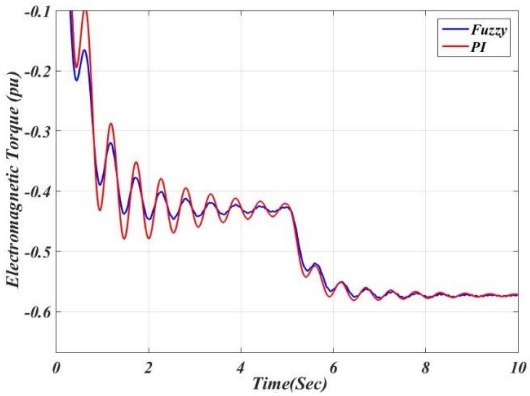

Figure 32. Electromagnetic torque-PI vs FLC for change in wind speed

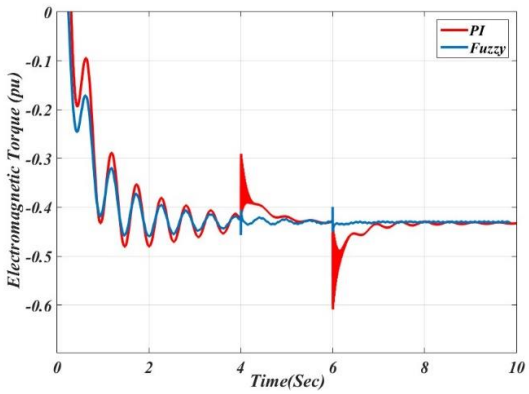

Figure 33. Variation of Electromagnetic torque for a grid voltage drop (wind speed-7 m/s)

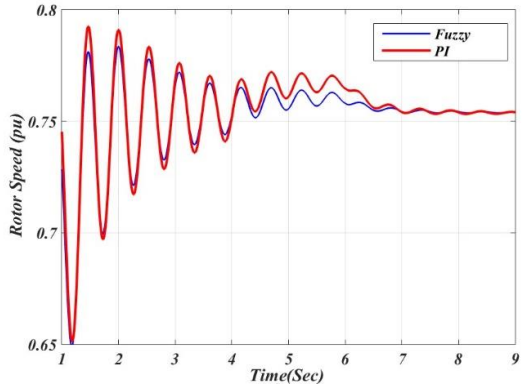

Figure 34. Variation of rotor speed for a grid voltage drop (wind speed- 7m/s)

From these simulation results, it has been observed that under fast dynamic conditions, the proposed FLC shows the better system performance compared to conventional PI controllers.
In DFIG based WPPs, RSC-GSC converters are controlled for grid synchronization and the active - reactive power control. This chapter proposes an additional decoupled control responsibility for RSC-GSC controllers for damping oscillations due to SSR frequencies. This eliminates the use of additional SSRDC and controller interactions.

A fuzzy based RSC controller is designed to damp SSR oscillations and the performance of the system with the proposed controller is tested. It has been observed that the proposed controller is very effective in damping SSR oscillations under fast dynamic conditions compared to conventional PI controllers. Also, the existing control technique for RSC in DFIG can be easily modified to suggested technique to damp out SSR oscillations and hence a separate SSRDC in addition to DFIG's own converter is eliminated in this model.

Conclusion

Series compensation gives rise to dynamic instability and subsynchronous resonance in the system. In this paper, the detailed SSR analysis of 2MW grid connected DFIG based windfarm was conducted by developing a detailed mathematical model of the system including the RSC-GSC dynamics for accurate analysis. The proposed model is found to be well suited for the small signal stability analysis. As the operating conditions like wind speed, compensation levels of transmission line etc., are varied, some oscillating modes become unstable and the work proposed the development of Fuzzy based controller for the RSC to damp SSR oscillations together with its own control responsibilities. So this proposed controller can be used to regulate the real and reactive power as the system requirement changes and also damps out the oscillations due to SSR. This is a novel effective solution for damping SSR oscillations because a separate SSRDC is not used which can reduce the total cost and complexity of the system control design. To extend this work, RSC-GSC converters of DFIG can be replaced with matrix converter and development of controllers that can adapt to the system changes can improve the system performance.

References

[1] J. G. Slootweg, and W. L. King, "Is the Answer Blowing in the Wind? ,"*IEEE Trans. Power & Energy Magazine*, vol. 3, pp. 26-33, Nov./ Dec. 2003.

[2] Indian Wind Energy Association. [Online] http://www.inwea.org/

[3] Global Wind Energy Council. [Online] http://www.gwec.net/

[4] World Energy Council. [Online] http://www.worldenergy.org/

[5] Ahmed Ewais, "The Effect of Wind Turbines on Subsynchronous Resonance, School of Engineering," Ph.D Dissertation , Cardiff University, UK, 2014.

[6] T. Ackermann, "Wind Power in Power Systems," John Wiley & Sons, England,2005.

[7] IEEE SSR Task Force, "Terms, Definitions and Symbols for Subsynchronous Oscillations," *IEEE Trans. Power Appl. Syst. PAS-96*, pp. 1326–1334, 1997.

[8] P. Kundur, "Power System Stability and Control," The EPRI Power System Engineering Series, McGraw-Hill, Inc, New York, 1994.

[9] P. M. Anderson, B. L. Agrawal and J. E. Van Ness, "Sub Synchronous Resonance in Power Systems," New York: IEEE Press, pp. 1-269, 1990.

[10] K.R. Padiyar, "Analysis of Sub-Synchronous Resonance in Power Systems," Kluwer Academic Publishers (KAP), Boston 1999.

[11] Anusri Parol and K.C.Sindhu Thampatty, "Mathematical Modeling of the Squirrel Cage Induction Generator based Wind Farm for Sub-Synchronous Resonance Analysis," *Indian Journal of Science and Technology*, Vol. 9, Issue 38, October 2016.

[12] H. Khalilinia and J. Ghaisari, "Sub-synchronous resonance damping in series compensated transmission lines using a statcom in the common bus," *2009 IEEE Power & Energy Society General Meeting*, Calgary, AB, pp. 1-7, 2009.

[13] J. Adams, C. Carter, and S. Huang, "ERCOT Experience with SubSynchronous Control Interaction and Proposed Remediation," *Proc. 2012 IEEE PES Transm. Dis. Conf. Expo. (T&D)*, pp. 7-10, 2012.

[14] H. A. Mohammadpour, Y. J. Shin and E. Santi, "SSR analysis of a DFIG-based Wind Farm Interfaced with a Gate-Controlled Series Capacitor," *IEEE Applied Power Electronics Conference and Exposition - APEC 2014*, pp. 3110-3117, Fort Worth, TX, 2014.

[15] Z. Miao, L. Fan, D. Osborn and S. Yuvarajan, "Control of DFIG based Wind Generation to Improve Inter-Area Oscillation Damping," *2008 IEEE Power and Energy Society General Meeting - Conversion and Delivery of Electrical Energy in the 21st Century*, Pittsburgh, PA, pp. 1-7, 2008.

[16] H. A. Mohammadpour and E. Santi, "SSR Damping Controller Design and Optimal Placement in Rotor-Side and Grid-Side Converters of SeriesCompensated DFIG-Based Wind Farm," *IEEE Transactions on Sustainable Energy*, vol. 6, no. 2, pp. 388-399, April 2015.

[17] 92L. Fan and Z. Miao, "Mitigating SSR using DFIG-based Wind Generation," IEEE Trans. Sustain. Energy, vol. 3, no. 3, pp. 349–358, Jul.2012.